Chinese Journal of Natural Medicines

Withanolide derivatives from *Physalis angulata* var. *villosa* and their cytotoxic activities

Peng Wang, Jue Yang, Yu Zhang, Jun Jin, Meijun Chen, Xiaojiang Hao, Chunmao Yuan, Ping Yi

Citation: Peng Wang, Jue Yang, Yu Zhang, Jun Jin, Meijun Chen, Xiaojiang Hao, Chunmao Yuan, Ping Yi, Withanolide derivatives from *Physalis angulata* var. *villosa* and their cytotoxic activities, Chinese Journal of Natural Medicines, 2025, 23(6), 762–768. doi: 10.1016/S1875–5364(25)60881–8.

View online: https://doi.org/10.1016/S1875–5364(25)60881–8

Chinese Journal of Natural Medicines 23 (2025) 762-768

Contents lists available at ScienceDirect

Chinese Journal of Natural Medicines

journal homepage: www.cjnmcpu.com/

Original article

Withanolide derivatives from *Physalis angulata* var. *villosa* and their cytotoxic activities

Peng Wang[a,b,c,Δ], Jue Yang[a,b,c,Δ], Yu Zhang[a,b,c], Jun Jin[a,b,c], Meijun Chen[a,b,c], Xiaojiang Hao[a,b,c,d], Chunmao Yuan[a,b,c,*], Ping Yi[a,b,c,*]

[a] *State Key Laboratory of Functions and Applications of Medicinal Plants, Guizhou Medical University, Guiyang 550014, China*
[b] *School of Pharmaceutical Sciences, Guizhou Medical University, Guiyang 561113, China*
[c] *Natural Products Research Center of Guizhou Province, Guiyang 550014, China*
[d] *Key Laboratory of Phytochemistry and Natural Medicines, Kunming Institute of Botany, Chinese Academy of Sciences, Kunming 650201, China*

ARTICLE INFO

Article history:
Received 3 July 2024
Revised 17 October 2024
Accepted 28 January 2025
Available online 20 July 2025

Keywords:
Physalis angulata var. *villosa*
Withanolide derivatives
Isolation and identification
Anti-cancer

ABSTRACT

A comprehensive phytochemical investigation of the leaves and twigs of *Physalis angulata.* var. *villosa* resulted in the isolation of 23 withanolide derivatives, including one novel 13,20-γ-lactone withanolide derivative (**1**) and three new withanolide derivatives (**2**–**4**). Architecturally, physalinin A (**1**) represents the first identified type B withanolide featuring a 13,20-γ-lactone moiety. The molecular structures of all isolates were elucidated using an integrated approach combining nuclear magnetic resonance (NMR) spectroscopy, mass spectrometry (MS), infrared (IR) spectroscopy, and quantum chemical calculations to confirm structural assignments. The antiproliferative activities of all isolated withanolides were evaluated against four human cancer cell lines (HEL, HCT-116, Colo320DM, and MDA-MB-231). Among them, eight derivatives (**2**, **5**–**8**, **14**, **15**, and **23**) exhibited significant inhibitory effects, with half-maximal inhibitory concentration (IC_{50}) values of 0.18 ± 0.03 to 17.02 ± 0.21 μmol·L^{-1}. Structure-activity relationship (SAR) analysis suggested that the presence of an epoxide ring enhances anticancer activity, potentially through increased reactivity or specific interactions with molecular targets involved in cancer progression. These findings underscore the pharmacological potential of withanolides as promising lead compounds for the development of novel anticancer therapeutics.

1. Introduction

Cancer remains one of the most prevalent diseases worldwide, with an estimated 10 million deaths reported in 2020, according to the World Health Organization (WHO). Despite the availability of numerous anticancer drugs, many exhibit severe side effects, necessitating the continued development of novel therapeutic agents with improved efficacy and safety profiles. Natural products derived from plants, animals, and microorganisms have historically served as a rich source of bioactive compounds in drug discovery, including agents with potent anticancer properties [1].

Withanolides are a class of polyoxygenated steroids characterized by an ergostane skeleton and are predominantly found in plants of the Solanaceae family. To date, over 300 withanolide derivatives have been identified, which can be broadly classified into two structural types based on the size and nature of the lactone or lactol ring at the side chain: type A (a δ-lactone or δ-lactol ring on the side chain) and type B (a γ-lactone or γ-lactol) [2]. Several withanolide derivatives, including physalins A, B, and F, have demonstrated potent cytotoxic activity [2], highlighting their potential as promising lead compounds for anticancer drug development.

Physalis angulata var. *villosa* (Solanaceae) is an annual herb widely distributed across tropical and temperate regions of the Americas. In traditional Chinese medicine, this species has long been used for the treatment of upper respiratory infections, sore throat, oral inflammation, jaundice associated with damp-heat, and dysentery [3-6]. In addition to its medicinal value, the plant's fruits are edible. In a previous investigation, we isolated 26 withanolide derivatives from the fruits of *P. angulata* var. *villosa*, many of which exhibited significant cytotoxic and anti-inflammatory activities [7]. Building on these findings, the present study undertook a comprehensive phytochemical investigation of the ethanol extract obtained from the aerial parts (leaves and stems) of *P. angulata* var. *villosa*. This led to the isolation of 23 structurally diverse withanolide derivativesl. Furthermore, their antiproliferative activities were assessed against four human cancer cell lines. Herein, we report the isolation, structural characterization, and biological evaluation of these withanolide derivatives.

2. Results and discussion

The structures of the 23 withanolide derivatives (Fig. 1), including two rare withanolide derivatives (**1** and **3**) and two new

* Corresponding author.
E-mail addresses: yuanchunmao01@126.com (C. Yuan); yiping2100@aliyun.com (P. Yi)
Δ These authors contributed equally to this work.

https://doi.org/10.1016/S1875-5364(25)60881-8

derivatives (**2** and **4**), were obtained from the aerial part of title plant. Nineteen known withanolide derivatives (**5**–**23**), physagulin C (**5**) [8], physangunolide B (**6**) [9], physagulide Q (**7**) [10], physagulide I (**8**) [11], physagulin K (**9**) [12], physagulide H (**10**) [13], physangulatin H (**11**) [14], physagulin Q (**12**) [15], physagulin L (**13**) [16], physagulin N (**14**) [12], 3α-methoxy-4β-hydroxy-physagulin N (**15**) [17], withaphysalin Z (**16**) [14], physangulatin G (**17**) [14], 25-OH-physalin F (**18**) [18], physalin G (**19**) [19], 5β-hydroxy-6α-chloro-5,6-dihydrophysalin B (**20**) [20], physaminin B (**21**) [21], physalin III (**22**) [18], and (22*R*)-5β,6β:14α,17:14β,26-triepoxy-2α-ethoxy-13,20,22-trihydroxy-1,15-dioxo-16α,24-cyclo-13,14-secoergosta-18,27-dioic acid 18→20, 27→22-dilactone (**23**) [22], were determined through detailed analysis of their nuclear magnetic resonance (NMR) spectroscopic data, which were compared with previously reported values in the literature.

Physalinin A (**1**) was isolated as a white powder, and its molecular formula $C_{28}H_{36}O_7$ was deduced from high-resolution electrospray ionization mass spectrometry (HR-ESI-MS) spectrum at *m/z* 507.2355 $[M + Na]^+$ (Calcd. for $C_{28}H_{36}O_7Na$, 507.2353), indicating 10 degrees of unsaturation. The ultraviolet (UV) spectrum exhibited a strong absorption at 220 nm, indicating the presence of an α,β-unsaturated carbonyl system, while the IR spectrum revealed the presence of hydroxy (3446 cm^{-1}) and α,β-unsaturated ketone (1631 cm^{-1}) groups. Its ^1H NMR spectrum (Table 1) displayed the existence of three methyls [δ_H 1.04 (d, J = 7.4 Hz, H_3-27), 1.15 (s, H_3-19) and 1.24 (s, H_3-21)] and three olefinic protons [δ_H 5.61 (1H, d, J = 6.0 Hz, H-6), 5.80 (1H, dd, J = 10.0, 3.0 Hz, H-2), and 6.93 (1H, m, H-3)]. The ^{13}C NMR spectrum (Table 2) displayed 28 carbon resonances, which were classified by an heteronuclear single quantum coherence (HSQC) spectroscopy as follows: three carbonyls [δ_C 176.9 (C-18), 179.8 (C-26), and 203.3 (C-1)], four olefinic carbons [δ_C 124.3 (C-6), 126.8 (C-2), 135.1 (C-5), and 147.1 (C-3)], four oxygenated carbons [δ_C 71.1 (CH_2-28), 71.8 (CH-22), 82.7 (C-14), and 85.9 (C-20)], and three methyl carbons [δ_C 10.1 (C-27), 18.4 (C-19), and 24.2 (C-21)]. The characteristic signals for two singlet methyls, a doublet methyl, and a γ-lactone ring implied that **1** was a type-B withanolide derivative [23, 24].

The 1D NMR data of **1** closely resembled those of perulactone B [25]. However, distinct structural differences were evident, notably the absence of hydroxyl substituents at C-17 and C-20 and the presence of an additional lactone ring bridging C-18 and C-20. The formation of this lactone ring was strongly supported by key heteronuclear multiple bond correlations (HMBCs) (Fig. 2), particularly from H-17 to C-13 and C-18, and from the methyl protons of H_3-21 to both C-20 and C-17. The characteristic γ-lactone ring chemical shifts at δ_C 176.9 (C-18) and δ_C 85.9 (C-20) further substantiated this assignment.

The relative configuration of compound **1** was established determined through nuclear Overhauser effect spectroscopy

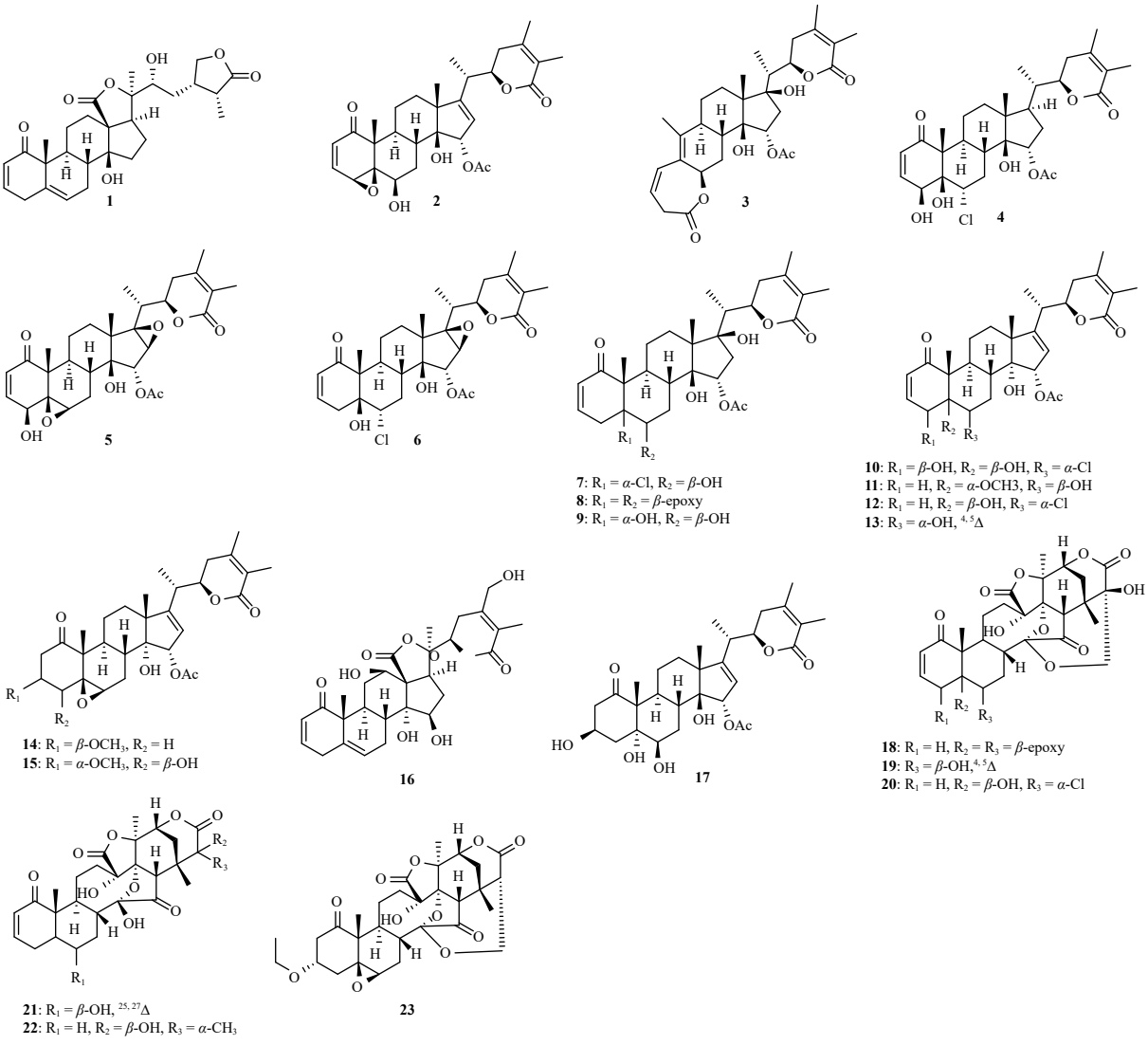

Fig. 1 Chemical structures of **1**–**23**.

(NOESY) correlations (Fig. 3). Cross-peaks of H-9/H-12α, H-12α/H-17, H-17/Me-21, Me-21/OH-22, Me-21/H-23α, and H-23α/Me-27 implied that the orientations of those groups were identical and adopted as α-oriented. Thus, H-25 was inferred to be β-oriented. The NOESY correlations of Me-19/H-8, H-8/OH-14, OH-14/H-22, H-22/H-24, and H-24/H-25 further corroborated the β-orientation of this set of protons. Thus, these NOESY correlations enabled a comprehensive and consistent assignment of the relative stereochemistry of **1**.

An electric circular dichroism (ECD) calculation was performed to establish the absolute configuration of **1** (Fig. 4) [7]. Two plausible stereoisomeric models were considered: (8*R*,9*S*,10*R*,13*S*,14*S*,17*S*,20*R*,22*R*,25*R*)-**1** and (8*S*,9*R*,10*S*,13*R*,14*R*,17*R*,20*S*,22*S*,25*S*)-**1**d. The calculated ECD spectrum of the former showed excellent agreement with the experimentally obtained ECD curve, thereby unambiguously establishing the absolute configuration of **1** as 8*R*,9*S*,10*R*,13*S*,14*R*,17*S*,20*R*,22*R*,25*R* (Fig. 4). To the best of our knowledge, this is the first example of a type-B withanolide derivative with a rare 18,20-γ-lactone ring.

The molecular formula of **2** was confirmed to be $C_{30}H_{38}O_8$ based on HR-ESI-MS (*m/z* 549.2459 [M + Na] (Calcd. for 549.2459). Comparison of the ^{1}H (Table 1) and ^{13}C NMR (Table 2) spectra of **2** with those of **16** [14] revealed close structural similarity, except for distinct differences observed in ring A. Specifically,

Table 1 ^{1}H NMR spectroscopic data for compounds **1**–**4** (*J* in Hz).

No.	1[a]	1[b]	2[a]	2[b]	3[b]	4[b]
2	5.9 (dd, 10.0, 3.0)	5.80 (dd, 10.0, 3.0)	5.98 (dd, 9.7, 2.0)	5.96 (dd, 9.7, 4.4)		5.86 (dd, 10.2, 2.0)
2α					2.96 (m)	
2β					4.09 (m)	
3	6.81 (m)	6.93 (m)	6.98 (dd, 9.7,2.0)	7.18 (dd, 9.7, 4.4)	5.51 (m)	6.47 (dd, 10.2, 2.0)
4			3.18 (m)	3.45 (m)	6.54 (dd,11.3, 3.3)	
4α	2.85 (m)	2.87 (m)				4.67 (m, H-4)
4β	3.3 (m)	3.30 (m)				5.7 (d, 7.0, OH-4)
5						4.48 (s, OH-5)
6	5.6 (d, 6.0)	5.61 (d, 6.0)	3.58 (t, 2.9)	3.47 (m, H-6); 5.22 (d, 3.4, OH-6)	5.29 (m)	4.24 (dd, 12.7, 4.7)
7α	1.78 (m)	1.66 (m)	2.31 (m)	2.14 (m)	1.43 (m)	1.69 (m)
7β	2.28 (m)	2.22 (m)	1.5 (m)	1.40 (m)	2.25 (m)	2.51 (m)
8	1.92 (m)	1.86 (m)	2.17 (m)	2.05 (m)	1.71 (m)	1.82 (m)
9	1.91 (m)	1.70 (m)	1.84 (m)	1.86 (m)	2.53 (m)	1.85 (m)
11	2.00, 2H					1.03 (m, 2H)
11α		1.84 (m)	1.27 (m)	1.00 (m)	1.97 (m)	
11β		1.90 (m)	1.35 (m)	1.27 (m)	1.17 (m)	
12						1.53 (m, 2H)
12α	1.66 (m)	1.59 (m)	1.79 (m)	1.72 (m)	1.52 (m)	
12β	2.13 (m)	1.98 (m)	1.35 (m)	1.20 (m)	1.63 (m)	
14		4.84 (s, OH-14)		4.47 (s, OH-14)	5.40 (s, OH-14)	4.59 (s, OH-14)
15	1.79, 2H		5.24 (d, 2.7)	5.08 (d, 2.7)	5.0 (m)	4.83 (d, 4.4)
15α		1.50 (m)				
15β		1.72 (m)				
16			5.6 (d, 2.6)	5.51 (d, 2.6)		
16α	1.82 (m)	1.73 (m)			2.53 (m)	1.60 (m)
16β	2.07 (m)	1.92 (m)			1.82 (m)	1.88 (m)
17	2.47 (m)	2.34 (m)			4.89 (s, OH-17)	1.49 (m)
18			1.19 (s)	0.98 (s)	1.03 (s)	0.96 (s)
19	1.28 (s)	1.15 (s)	1.37 (s)	1.32 (s)	1.77 (s)	1.03 (s)
20			2.53	2.45 (m)	2.05 (m)	1.86 (m)
21	1.39 (s)	1.24 (s)	1.07 (d, 7.0)	1.06 (d, 7.0)	0.96 (d, 7.0)	0.88 (d, 6.5)
22	3.97 (d, 9.7)	3.79 (m); 5.08 (d, 4.9, OH-22)	4.29 (m)	4.29 (m)	4.70 (m)	4.32 (m)
23					2.41 (m, 2H)	
23α	1.52 (m)	1.45 (m)	2.36 (m)	2.49 (m)		2.38 (m)
23β	1.38 (m)	1.09 (m)	2.25 (m)	2.14 (m)		2.00 (m)
24	2.68 (m)	2.60 (m)				
25	2.70 (m)	2.70 (m)				
26						
27	1.18 (d, 7.4)	1.04 (d, 7.4)	1.84 (s)	1.78 (s)	1.73 (s)	1.72 (s)
28		4.29 (m, 2H)	1.94 (s)	1.88 (s)	1.89 (s)	1.88 (s)
28α	4.29 (m)					
28β	4.43 (m)					
30			1.91 (s)	1.89 (s)	1.97 (s)	1.98 (s)

[a] Recorded in $CDCl_3$; [b] Recorded in DMSO-d_6.

2 exhibited a $^{2,3}\Delta$ double bond and a 4,5-epoxy ring that were absent in **16**. In the 1D NMR spectra (Table 1), the proton signals at δ_H 5.96 (1H, dd, *J* = 9.7, 2.0 Hz, H-2) and 7.18 (1H, dd, *J* = 9.7, 2.0 Hz, H-3) combined with the signals at δ_C 199.6 (C-1), 129.2 (C-2), and 143.0 (C-3) in the ^{13}C NMR spectrum are characteristic of an *α*,*β*-unsaturated enone system. Moreover, the typical chemical shifts [δ_H 3.45 (1H, m, H-4); δ_C 52.1, and 65.7] implied the presence of an epoxy ring between C-4 and C-5. This substitution pattern was further confirmed by the HMBCs of H_3-19 with C-1, C-5, C-9 and C-10, and of H-6 with C-4 and C-5 (Fig. 2). The ^{1}H–^{1}H correlation spectroscopy (COSY) correlations (Fig. 2) of H-3 with H-4 provided further support for the substitution pattern within ring A. Therefore, the above data confirmed the gross structure of **2**.

The relative configuration of **2** was established through the NOESY spectrum (Fig. 3). Cross-peaks of Me-18/OH-14, Me-18/H-20, OH-14/H-15, OH-14/H-8, H-8/OH-6, and H-8/Me-19 implied that the orientations of those groups were identical and adopted as *β*-oriented. Conversely, NOESY correlations (Fig. 3) of H-6 to H-4 and H-9, and of Me-21 to H-22 indicated that those protons were *α*-orientated. ECD calculation method was conducted to determine the absolute configuration. The calculated ECD curve for the 4*S*,5*S*,6*R*,8*R*,9*S*,10*R*,13*R*,14*S*,15*S*,20*S*,22*R* tereoisomer was in excellent agreement with the experimental data (Fig. 4), thereby confirming the absolute configuration of **2**.

The molecular formula of physalinin C (**3**) was deduced to be $C_{30}H_{40}O_8$ based on the HR-ESI-MS data (*m/z* 551.2606 [M + Na]$^+$, Calcd. for 551.2615). Comparison of the ^{1}H and ^{13}C NMR signals of **3** with those of physalane B [26] indicated a shared carbon skeleton and stereochemistry. The obvious difference between the two compounds was the presence of the hydroxy group of C-17 in **3** (Tables 1 and 2), verified by HMBCs of OH-17 with C-16, C-17, and C-20. Additionally, NOESY correlations (Fig. 3) of OH-17 with Me-18 and OH-14, and OH-14 with H-15, indicated that these protons were *β*-orientated. The spectral evidence allowed for the definitive structural and stereochemical assignment of **3** as physalinin C.

The HR-ESI-MS data of physalinin E (**4**) afforded the molecular formula, $C_{30}H_{41}ClO_8$ ([M + Na]$^+$ 587.2383; Calcd. for $C_{30}H_{40}O_7Na$, 587.2382), indicating two additional mass units relative to **10**. Comparison of the NMR data between compounds **4** and **10** indicated that both compounds shared the similar structure, with the key distinction being the absence of a $^{16,17}\Delta$ double bond in **4**. This conclusion was testified by the ^{1}H–^{1}H COSY correlations of H-15/H_2-16/H-17/H-20/H-22/H_2-23 and HMBC correlations from Me-21 and Me-18 to C-17 (δ_C 52.3) (Fig. 2). Thus, the planner structure was assigned.

A NOESY experiment (Fig. 3) was performed to elucidate the relative configuration of **4**. A significant downfield shift in the chemical shift of C-15 (δ_C 79.5 in **4** *vs* 83.9 in **10**) indicated a configurational change. NOESY cross-peaks between OH-14 and both Me-18 and H-15 confirmed the *β*-orientation of OH-14 and H-15. Additionally, NOESY correlations of H-17 with Me-21 and H-22 established the *α*-orientation of H-17 (Fig. 3). Based on the collective spectroscopic evidence, the complete structure and ste-

Table 2 ^{13}C NMR spectroscopic data for compounds **1**–**4**.

No.	1[a]	1[b]	2[a]	2[b]	3[b]	4[b]
1	204.1	203.3	198.8	199.6	172.2	200.7
2	127.8	126.8	130.3	129.2	35.3	125.6
3	145.8	147.1	141.3	143.0	118.3	146.6
4	33.4	32.7	52.3	52.1	128.6	63.7
5	135.5	135.1	66.3	65.7	124.8	78.5
6	124.3	124.3	72.7	71.1	72.5	64.7
7	26.6	26.1	31.7	31.5	27.1	34.0
8	40.0	38.8	34.5	34.9	38.1	40.5
9	38.2	37.7	42.6	42.0	41.2	40.6
10	51.5	50.6	52.6	50.4	142.1	57.1
11	23.0	22.9	21.5	21.1	24.3	22.3
12	35.1	34.52	38.1	37.5	31.0	41.9
13	61.3	59.4	52.3	52.1	50.3	46.0
14	83.9	82.7	82.2	80.2	84.6	82.8
15	34.6	34.46	83.6	83.0	79.3	79.5
16	24.6	24.2	120.5	121.3	47.1	33.8
17	56.7	56.2	161.4	160.9	85.1	51.3
18	178.0	176.9	16.6	15.7	15.0	17.2
19	18.9	18.4	13.5	12.7	15.3	8.4
20	87.3	85.9	35.7	34.1	41.2	37.3
21	24.5	24.2	17.0	17.4	9.5	14.7
22	73.5	71.8	78.3	78.0	76.2	77.8
23	29.4	29.5	32.2	31.5	31.6	29.9
24	38.1	38.2	151.0	150.4	150.7	150.5
25	38.0	37.4	121.5	120.3	120.3	120.3
26	180.2	179.8	167.9	165.8	166.0	165.9
27	10.7	10.1	12.5	12.3	12.2	12.3
28	72.2	71.1	20.5	20.1	20.3	20.2
29			169.6	169.3	169.3	169.2
30			21.4	21.1	21.2	21.3

[a] Recorded in $CDCl_3$; [b] Recorded in DMSO-d_6.

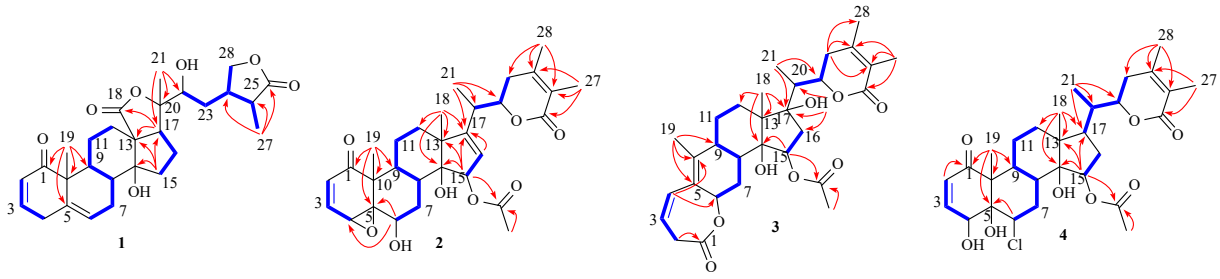

Fig. 2 Key HMBC (⟶) and $^{1}H-^{1}H$ COSY (▬) correlations of **1**–**4**.

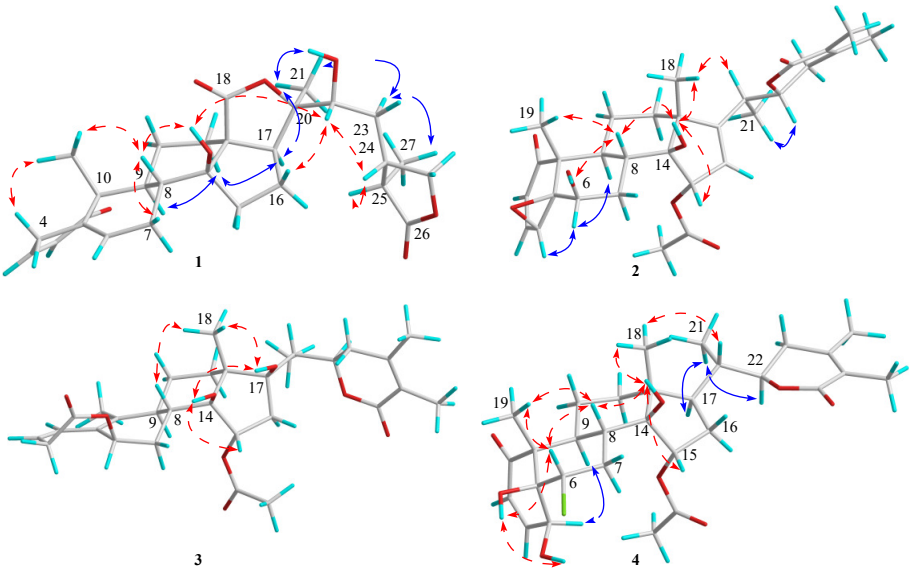

Fig. 3 NOESY (⇢) correlations of **1**–**4**.

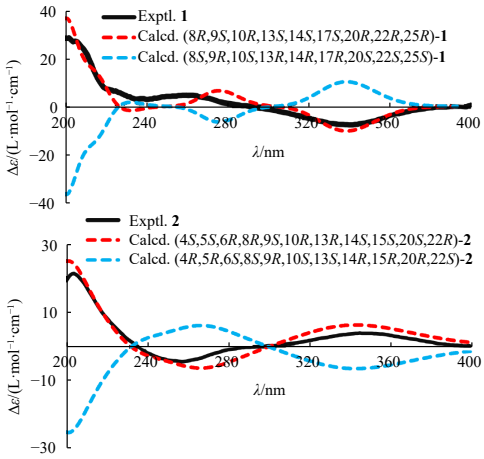

Fig. 4 Experimental and calculated ECD spectra of **1** and **2**.

reochemistry of physalinin E (**4**) were unambiguously assigned.

2.1. Cytotoxic activity

The antiproliferative activities of all isolated compounds were evaluated against four human cancer cell lines (HEL, HCT-116, Colo320DM, and MDA-MB-231) using MTT assay as previously described [24, 25]. Of the 23 compounds tested, eight (**2**, **4**–**5**, **7**–**8**, **14**, **15**, and **23**) exhibited good cytotoxic activities on cancer cells, with half-maximal inhibitory concentration (IC_{50}) values ranging from 0.18 ± 0.03 to 17.02 ± 0.21 μmol·L^{-1} (Table 3). Among them, compound **5** showed the strongest cytotoxic activity against HEL and HCT-116, with IC_{50} value of 0.18 ± 0.03 and 1.37 ± 0.13 μmol·L^{-1}, respectively. Additionally, compounds **5**, **7**, and **8** displayed superior cytotoxic potency against Colo320DM cells than the positive control, adriamycin, with compound **8** exhibiting the highest activity (1.77 ± 0.22 μmol·L^{-1}).

The structure-activity relationship (SAR) analysis revealed that withanolide derivatives (**4**–**9**), which lack a $^{16,17}\Delta$ double bond, exhibited notable cytotoxic activity, except for compounds **6** and **9**. Moreover, compound **5** with two epoxide rings exhibited the most potent cytotoxic effects against HCT-116 and HEL. In contrast, compounds **14** and **15**, containing only one epoxide ring, also displayed cytotoxic activity against HEL cells, but their potency was lower than that of compound **5**. Among the physalin derivatives (**18**–**23**), only compound **23**, which contains a single epoxide ring, exhibited cytotoxic activity. These findings suggest the epoxide ring and the saturation of the C-16/C-17 bond as key pharmacophores influencing anticancer activity in this class of withanolides.

3. Conclusion

A total of 23 withanolide derivatives were isolated from the stems and leaves of *P. angulata* var. *villosa*, including a novel 13,20-γ-lactone withanolide (**1**) and three previously unreported withanolide derivatives (**2**–**4**). Structurally, physalinin A (**1**) represents the first identified type-B withanolide featuring a 13,20-γ-lactone moiety, while physalinin C (**3**) is a rare rearranged 1,10-secowithanolide with a tetracyclic 7/6/6/5 ring system. Eight of the isolated compounds demonstrated significant cytotoxic activity against four tumor cell lines, with IC_{50} values ranging from 0.18 ± 0.03 to 17.02 ± 0.21 μmol·L^{-1}. SAR analysis indicated that

Table 3 Cytotoxic activities of compounds **1**–**23** [a] (mean ± SD, n = 3).

Com.	IC_{50}/(μmol·L^{-1})			
	HEL	HCT-116	Colo320DM	MDA-MB-231
2	17.02 ± 0.21	7.66 ± 0.25	8.27 ± 0.16	8.79 ± 0.25
4	16.97 ± 0.11	> 20	> 20	> 20
5	0.18 ± 0.03	1.37 ± 0.13	2.12 ± 0.31	3.57 ± 0.35
7	1.64 ± 0.12	2.51 ± 0.25	2.11 ± 0.08	3.60 ± 0.18
8	1.17 ± 0.17	2.14 ± 0.31	1.77 ± 0.22	> 20
14	12.16 ± 0.23	11.96 ± 0.22	11.28 ± 1.36	> 20
15	9.70 ± 1.02	> 20	> 20	> 20
23	9.35 ± 0.66	9.03 ± 0.33	12.76 ± 0.53	> 20
ADR [b]	0.15 ± 0.09	1.20 ± 0.07	5.81 ± 0.34	0.82 ± 0.15

[a] Other compounds (**1**, **3**, **6**, **9**–**13**, and **16**–**22**) were inactive at the concentration of 20 μmol·L^{-1}; [b] ADR: adriamycin is used as a positive control.

the presence of an epoxide ring plays a key role in enhancing anticancer activity. In particular, compound **5**, which contains two epoxide rings, exhibited the highest cytotoxic activity against HEL and HCT-116 cells (IC_{50} 0.18 ± 0.03 and 1.37 ± 0.13 μmol·L^{-1}, respectively).

4. Experimental

4.1. General information

Petroleum ether, dichloromethane, ethyl acetate, acetone, methanol, high-performance liquid chromatography (HPLC)-grade methanol (MeOH), and acetonitrile (ACN) were purchased from Shanghai Wohua Chemical Corporation (Shanghai, China). We bought fetal bovine serum (FBS) along with Dulbecco's modified Eagle's medium (DMEM) from Gibco Invitrogen Corporation (Carlsbad, USA). 3-(4,5-Dimethylthiazol-2-yl)-2,5-diphenyl tetrazolium bromide (MTT) and dimethyl sulfoxide (DMSO) were purchased from Sigma-Aldrich (St. Louis, MO, USA).

UV spectra, infrared (IR) spectra, optical rotations, and ECD data were tested on a Shimadzu UV-2401PC spectrometer (Tokyo, Japan), Nicolet Nexus 470 spectrophotometer (KBr disks) (Massachusetts, USA), an Autopol IV automatic (Hackettstown, USA), and a JASCO-810 polarimeter (Tokyo, Japan), respectively. NMR spectra and HR-ESI-MS were recorded on a Bruker Advance NEO 600 spectrometer (Billerica, USA) and Thermo Ultimate 3000/Q EXACTIVE FOCUS mass spectrometer (Waltham, MA, USA), respectively. Semi-preparative HPLC separation was conducted on Hanbon NS4210 (Jiangsu, China) equipped with a YMC-C_{18} column (250 mm × 10.0 mm, 5 μm). TLC (GF_{254}, Qingdao Marine Chemical Co., Ltd.) was used to detect fractions.

4.2. Plant material

The aerial parts of *P. angulata* var. *villosa* were collected from Yuping County, Guizhou Province of China and identified by Mr. Jun Zhang (Yunnan Plant Pharmaceutical Biotechnology Co., Ltd.). A voucher specimen (No. 20211015) was deposited at the Natural Products Research Center of Guizhou Province.

4.3. Extraction, isolation, and purification

The dried aerial parts of *P. angulata* var. *villosa* (40.0 kg) were pulverized and extracted with ethanol at 25 °C. Following evaporation under reduced pressure, the crude extract (1.6 kg) was subjected to silica gel column chromatography using a petroleum ether–acetone gradient system (95∶5 to 30∶70), affording six fractions (Frs. 1–6).

Fr. 3 (600.0 g) was further purified using an MCI-gel column with MeOH/H_2O (from 4∶6 to 10∶0), yielding eight subfractions (Fr. 3A–3H). Fr. 3G (80.0 g) was subjected to silica gel chromatography using CH_2Cl_2–EtOAc (from 99∶1 to 95∶5), affording three fractions (Frs. 3G.A–C) Fr. 3G.B (22.0 g) was further purified on Sephadex LH-20 (MeOH) and silica gel column to obtain **6** (5.0 mg), **5** (9.3 mg), **7** (23.0 mg), **8** (200.0 mg), **9** (50.0 mg), and **23** (12.3 mg, methanol crystallization).

Fr. 3E was purified by silica gel column washed with dichloromethane/acetone (*V*/*V*, 9∶1–6∶4), yielding four fractions (Frs. 3E1–3E3). Compounds **1** (22.6 mg, t_R 24 min, ACN–H_2O, 38∶62) and **17** (t_R 22 min, MeOH–H_2O, 57∶43) were purified by the semi-preparative HPLC for Frs. 3E1 and 3E2, respectively. Compounds **14** (300 mg) and **15** (8.3 mg) were obtained from Fr. 3E3 *via* silica gel chromatography (petroleum ether/ethyl acetate, 7∶3).

Fraction 3F (10.3 g) was subjected to silica gel column chromatography using petroleum ether–acetone (9∶1 to 1∶1, *V*/*V*), affording compounds **2** (6.3 mg), **3** (10.6 mg), **11** (3.6 mg), **12** (3.3 mg), and **13** (700 mg). Compounds **4** (8.2 mg, t_R 24 min) and **10** (20 mg, t_R 36 min) were purified from Fr. 3C5 (8.6 g) using the semi-preparative HPLC (MeOH–H_2O, 61∶39, *V*/*V*).

Fr. 3D (6.2 g) was purified by a silica gel column washed with CH_2Cl_2/EtOAc (*V*/*V*, 9∶1–6∶4) to yielded four sub-fractions (Fr. 3D1–3D4). Four compounds, **18** (7.0 mg), **20** (5.7 mg), **21** (9.0 mg), and **16** (10.6 mg) were obtained from Fr. 3D1 (3.2 g) through a silica gel column (300–400 mesh) washed with CH_2Cl_2/EtOAc (*V*/*V*, 97∶3). Compounds **19** (3.6 mg, t_R 18 min, ACN–H_2O, 30∶70) and **22** (26.0 mg, t_R 9 min, MeOH–H_2O, 30∶70) were obtained by semi-preparative HPLC for Fr. 3D3 (1.6 g).

Physalinin A (**1**): white powder; $[\alpha]_D^{25}$ +26.9 (*c* 0.05, MeOH); UV (MeOH) (log ε) 220 (4.06) nm; IR (KBr) ν_{max} 3446, 2359, 1631, 1350 cm^{-1}; ^{1}H NMR ($CDCl_3$, 600 MHz), ECD (MEOH) λ_{max} ($\Delta\varepsilon$) 396 (+0.05), 341 (−6.69), 265 (+5.06), 200 (+19.9) nm, and ^{13}C NMR ($CDCl_3$, 150 MHz) data (Tables 1 and 2); (+)-HR-ESI-MS *m/z* 507.2355 $[M + Na]^+$ (Calcd. for $C_{30}H_{38}O_7Na$, 507.2353).

Physalinin B (**2**): white powder; $[\alpha]_D^{25}$ +119.7 (*c* 0.05, MeOH); UV (MeOH) λ_{max} (log ε) 230 (4.59) nm; IR (KBr) ν_{max} 3430, 1634, 1384, 1350 cm^{-1}; ^{1}H NMR ($CDCl_3$, 600 MHz), ECD (MeOH) λ_{max} ($\Delta\varepsilon$) 345 (+3.56), 252 (−2.96), 202 (+16.67) nm, and ^{13}C NMR ($CDCl_3$, 150 MHz) data (Tables 1 and 2); (+)-HR-ESI-MS *m/z* 549.2459 $[M + Na]^+$ (Calcd. for $C_{30}H_{40}O_7Na$, 549.2459).

Physalinin C (**3**): white powder; $[\alpha]_D^{25}$ +33.7 (*c* 0.04, MeOH); UV (MeOH) λ_{max} (log ε) 240 (3.98) nm; IR (KBr) ν_{max} 3440, 2358, 2342, 1631 cm^{-1}; ECD (MeOH) λ_{max} ($\Delta\varepsilon$) 282 (+0.17), 258 (+1.90), 221 (+7.72), 214 (+4.95), 209 (+5.60) nm, ^{1}H NMR ($CDCl_3$, 600 MHz) and ^{13}C NMR ($CDCl_3$, 150 MHz) data (Tables 1 and 2); (+)-HR-ESI-MS *m/z* 551.2606 $[M + Na]^+$ (Calcd. for $C_{30}H_{42}O_7Na$, 551.2615).

Physalinin D (**4**): white powder; $[\alpha]_D^{25}$ +100 (*c* 0.06, MeOH); UV (MeOH) λ_{max} (log ε) 215 (4.98) nm; IR (KBr) ν_{max} 3445, 2358, 1681, 1631, 1350 cm^{-1}; ^{1}H NMR ($CDCl_3$, 600 MHz) and ^{13}C NMR ($CDCl_3$, 150 MHz) data (Tables 1 and 2); (+)-HR-ESI-MS *m/z* 587.2383 $[M + Na]^+$ (Calcd. for $C_{30}H_{42}O_7Na$, 587.2382).

4.4. Theoretical ECD calculation

The two lowest-energy conformers were selected using the same computational methods employed for ^{13}C NMR chemical shift calculations. Each conformer was optimized using the polarizable continuum model (PCM) and subsequently analyzed *via* time-dependent density functional theory (TD-DFT) to obtain theoretical ECD spectra. The final ECD spectra were generated us-

ing SpecDis 1.71 (University of Würzburg, Würzburg, Germany) [26-30].

4.5. Cytotoxicity assay

The cytotoxicity assay was conducted using MTT assay, as described previously [31, 32]. Briefly, cancer cells were seeded into 96-well plates and incubated in a CO_2 incubator for 24 h. Following cell attachment, cells were treated with varying concentrations of the test compounds and further incubated for 72 h. Subsequently, MTT solution was added to each well, and absorbance was measured using a microplate reader (Varioskan LUX, Thermo, USA) to determine cell viability. The IC_{50} values were calculated based on dose-response curves. The initial screening concentration for all isolates was 20 μmol·L^{-1}. For active compounds, different concentrations of compounds, 20, 10, 5, 2.5, 1.25, 0.625, and 0.313 μmol·L^{-1}, were applied to calculate the IC_{50} values. All experiments were conducted in triplicate.

Funding

This work was supported by the National Natural Science oundation of China (Nos. 31960087, 82060631, and 32270413), the Science and Technology Department of Guizhou Province (No. QKHJC[2020]1Z076), the Excellent Young Talents Plan of Guizhou Medical University (2023, No.106), the 13th Batch of Outstanding Young Scientific and Technological Talents in Guizhou Province (No. QKHPTRC[2021]5633), the Natural Science Foundation of Guizhou Province (No. QKHZYD[2022]4015), the High-level Innovative Talents in Guizhou Province (Thousand Levels of Talent for Chunmao Yuan in 2018 and Jue Yang in 2023), 2022 Guiyang Science and Technology Talent Training Project (No. ZKH[2023]48-5), Guizhou Science and Technology Innovation Talent Team (No. QKHPTRC-CXTD[2022]007), and the "Light of the West" Talent Cultivation Program of Chinese Academy of Sciences for Chunmao Yuan (No. RZ[2020]82).

Availability of supporting information

Supporting information for this study can be obtained by contacting the corresponding authors *via* E-mail.

Declaration of competing interest

The authors declare that they have no known competing financial interests or personal relationships that could have appeared to influence the work reported in this paper.

References

1 Atanasov AG, Zotchev SB, Dirsch VM, et al. Natural products in drug discovery: advances and opportunities. *Nat Rev Drug Discov*. 2021;20:200-216. https://doi.org/10.1038/s41573-020-00114-z.
2 Xia GY, Cao SJ, Chen LX, et al. Natural withanolides, an update. *Nat Prod Rep*. 2022;39:784-813. https://doi.org/10.1039/D1NP00055A.
3 Cao CM, Wu X, Kindscher K, et al. Withanolides and sucrose esters from *Physalis neomexicana*. *J Nat Prod*. 2015;78(10):2488-2493. https://doi.org/10.1021/acs.jnatprod.5b00698.
4 Chen LX, Xia GY, He H, et al. New withanolides with TRAIL-sensitizing effect from *Physalis pubescens* L. *RSC Adv*. 2016;6:52925-52936. https://doi.org/10.1039/C6RA07031K.
5 He H, Zang LH, Feng YS, et al. Physalin A induces apoptosis *via* p53-Noxa-mediated ROS generation, and autophagy plays a protective role against apoptosis through p38-NF-κB survival pathway in A375-S2 cells. *J Ethnopharmacol*. 2013;148:544-555. https://doi.org/10.1016/j.jep.2013.04.051.
6 Qiu L, Zhao F, Jiang ZH, et al. Steroids and flavonoids from *Physalis alkekengi* var. *franchetii* and their inhibitory effects on nitric oxide production. *J Nat Prod*. 2008;71(4):642-646. https://doi.org/10.1021/np700713r.
7 Wang P, Yang XM, Hu ZX, et al. UPLC-Q-orbitrap-MS/MS-guided isolation of bioactive withanolides from the fruits of *Physalis angulata*. *J Agric Food Chem*. 2023;71(44):16581-16592. https://doi.org/10.1021/acs.jafc.3c04311.
8 Shingu K, Marubayashi N, Ueda I, et al. Physagulin C, a new withanolide from *Physalis angulata* L. *Chem Pharm Bull*. 1991;39(6):1591-1593. https://doi.org/10.1248/cpb.39.1591.
9 Zhang JF, Wu SF, Zhu L, et al. Withanolides from *Physalis angulata* var. *villosa* and the relative configurational revision of some known analogs. *J Nat Prod*. 2024;87(1):38-49. https://doi.org/10.1021/acs.jnatprod.3c00725.
10 Huang M, He JX, Hu HX, et al. Withanolides from the genus *Physalis*: a review on their phytochemical and pharmacological aspects. *J Pharm Pharmacol*. 2020;72(5):649-669. https://doi.org/10.1111/jphp.13209.
11 Tan YH, Cai YX, Kong M, et al. Withanolides from *Physalin angulata* and their inhibitory effects on nitric oxide production. *Chem Biodivers*. 2023;20(4):e202300195. https://doi.org/10.1002/cbdv.202300195.
12 Abe F, Nagafuji S, Okawa M, et al. Trypanocidal constituents in plants 6 minor withanolides from the aerial parts of *Physalis angulata*. *Chem Pharm Bull*. 2006;54(8):1226-1228. https://doi.org/10.1248/cpb.54.1226.
13 Ma T, Zhang WN, Yang L, et al. Cytotoxic withanolides from *Physalis angulata* var. *villosa* and the apoptosis-inducing effect *via* ROS generation and the activation of MAPK in human osteosarcoma cells. *RSC Adv*. 2016;6:53089-53100. https://doi.org/10.1039/C6RA08574A.
14 Sun CP, Qiu CY, Yuan T, et al. Antiproliferative and anti-inflammatory withanolides from *Physalis angulata*. *J Nat Prod*. 2016;79(6):1586-1597. https://doi.org/10.1021/acs.jnatprod.6b00094.
15 Ding H, Hu Z, Yu L, et al. Induction of quinone reductase (QR) by withanolides isolated from *Physalis angulata* L. var. *villosa* Bonati (Solanaceae). *Steroids*. 2014;86:32-38. https://doi.org/10.1016/j.steroids.2014.04.015.
16 Yen PH, Cuong LCV, Dat TTH, et al. Withanolides from the whole plant of *Physalis angulata* and their anti-inflammatory activitie. *Vietnam J Chem*. 2019;57(3):334-338. https://doi.org/10.1002/vjch.201900031.
17 Qiu F, Chen LX, Zhang M, et al. *Withanolide Compound and Its Application in Preparation of Drugs for Treating Tumor Diseases*. CN 111718393A. 2020-09-29.
18 Ozawa M, Morita M, Hirai G, et al. Contribution of cage-shaped structure of physalins to their mode of action in inhibition of NF-κB activation. *ACS Med Chem Lett*. 2013;4(8):730-735. https://doi.org/10.1021/ml400144e.
19 Chen R, Liang JY, Yang Y, et al. Chemical constituents from *Physalis alkekengi* and structural revision of physalin G. *Chin J Nat Med*. 2007;5(3):186-189.
20 Men RZ, Li N, Ding WJ, et al. Unprecedent aminophysalin from *Physalis angulata*. *Steroids*. 2014;88:60-65. https://doi.org/10.1016/j.steroids.2014.06.016.
21 Wu JP, Li LY, Li JR, et al. Silencing tautomerization to isolate unstable physalins from *Physalis minima*. *J Nat Prod*. 2022;85(6):1522-1539. https://doi.org/10.1021/acs.jnatprod.2c00101.
22 Li Y, Pan Y, Huang X, et al. Withanolides from *Physalis alkekengi* var. *francheti*. *Helv Chim Acta*. 2008;91(12):2284-2291. https://doi.org/10.1002/hlca.200890248.
23 Chen LX, He H, Qiu F. Natural withanolides: an overview. *Nat Prod Rep*. 2011;28(4):705-740. https://doi.org/10.1039/c0np00045k.
24 Silva EL, Almeida-lafetá RC, Borges RM, et al. Athenolide A, a new steroidal lactone from the leaves of *Athenaea martiana* (Solanaceae) determined by means of HPLC-HR-MS-SPE-NMR analysis. *Chem Biodivers*. 2018;15(1):e1700455. https://doi.org/10.1002/cbdv.201700455.
25 Fang ST, Liu JK, Li B. Ten new withanolides from *Physalis peruviana*. *Steroids*. 2012;77(1–2):36-44. https://doi.org/10.1016/j.steroids.2011.09.011.
26 Marcarino MO, Cicetti S, Zanardi MM, et al. A critical review on the use of DP4+ in the structural elucidation of natural products: the good, the bad and the ugly. A practical guide. *Nat Prod Rep*. 2022;39(1):58-76. https://doi.org/10.1039/D1NP00030F.
27 Xiao Y, Muhammad I, Ma X, et al. Camganoids A and B, two new sesquiterpenes with different carbon skeletons isolated from fruits of *Cinnamomum migao*. *Chin Herb Med*. 2022;14(4):638-642. https://doi.org/10.1016/j.chmed.2021.09.016.
28 Zanardi MM, Sarotti AM. Sensitivity analysis of DP4+ with the probability distribution terms: development of a universal and customizable method. *J Org Chem*. 2021;86(12):8544-8548. https://doi.org/10.1021/acs.joc.1c00987.
29 Xie S, Qi C, Duan Y, et al. Discovery of new polycyclic polyprenylated acylphloroglucinols with diverse architectures as potent cyclooxygenase-2 inhibitors. *Org Chem Front*. 2020;7:1349-1357. https://doi.org/10.1039/D0QO00259C.
30 Xin D, Jones PJ, Gonnella NC. DiCE: diastereomeric *in silico* chiral elucidation, expanded DP4 probability theory method for diastereomer and structural assignment. *J Org Chem*. 2018;83(9):5035-5043. https://doi.org/10.1021/acs.joc.8b00338.
31 Li Y, Qiu J, Yi P, et al. Isolation and synthesis of rocaglaol derivatives by inhibiting wnt/β-catenin and MAPK signaling pathways against colorectal cancer. *Bioorg Chem*. 2022;129:106149. https://doi.org/10.1016/j.bioorg.2022.106149.
32 Wang F, Hua H, Pei Y, et al. Triterpenoids from the resin of *Styrax tonkinensis* and their antiproliferative and differentiation effects in human leukemia hl-60 cells. *J Nat Prod*. 2006;69(5):807-810. https://doi.org/10.1021/np050371z.